Nanoscale Advances

ROYAL SOCIETY OF CHEMISTRY

PAPER

View Article Online
View Journal | View Issue

Cite this: *Nanoscale Adv.*, 2023, **5**, 2071

Sustained release of tumor cell lysate and CpG from an injectable, cytotoxic hydrogel for melanoma immunotherapy

Kui Yang,†[ab] Yuhan Zhou, †[ac] Biwang Huang,[d] Guifang Zhao,[ae] Yuan Geng,[f] Chao Wan,[a] Fagang Jiang,[g] Honglin Jin,[af] Chengzhi Ye*[h] and Jing Chen*[a]

Many basic research studies have shown the potential of autologous cancer vaccines in the treatment of melanoma. However, some clinical trials showed that simplex whole tumor cell vaccines can only elicit weak $CD8^+$ T cell-mediated antitumor responses which were not enough for effective tumor elimination. So efficient cancer vaccine delivery strategies with improved immunogenicity are needed. Herein, we described a novel hybrid vaccine "MCL" (Melittin–$RADA_{32}$–CpG–Lysate) which was composed of melittin, $RADA_{32}$, CpG and tumor lysate. In this hybrid vaccine, antitumor peptide melittin and self-assembling fusion peptide $RADA_{32}$ were assembled to form the hydrogel framework melittin–$RADA_{32}$(MR). Then, whole tumor cell lysate and immune adjuvant CpG-ODN were loaded into MR to develop an injectable and cytotoxic hydrogel MCL. MCL showed excellent ability for sustained drug release, to activate dendritic cells and directly kill melanoma cells *in vitro*. *In vivo*, MCL not only exerted direct antitumor activity, but also had robust immune initiation effects including the activation of dendritic cells in draining lymph nodes and the infiltration of cytotoxic T lymphocytes (CTLs) in tumor microenvironment. In addition, MCL can efficiently inhibit melanoma growth in B16–F10 tumor bearing mice, which suggested that MCL is a potential cancer vaccine strategy for melanoma treatment.

Received 13th December 2022
Accepted 24th February 2023

DOI: 10.1039/d2na00911k

rsc.li/nanoscale-advances

1 Introduction

Melanoma is a highly invasive cancer with rapid dissemination by lymph nodes and blood, and is not sensitive to conventional radiotherapy and chemotherapy.[1–5] Therefore, there is a need to explore new efficient treatment for melanoma. Immunotherapy is currently the most promising treatment for cancer, which mainly includes cytokine therapy, adoptive T-cell therapy, immune checkpoint inhibitors and tumor vaccines.[6–9] Autologous tumor vaccines can initiate immune response and subsequent T cell infiltration to achieve the anti-tumor effect, with individual specificity and slight systemic side effects.[10–13] However, existing tumor vaccines may have the following application defects. First, vaccines cannot inhibit the rapid tumor progression in early stages because of the lack of direct killing effect on tumor cells. The immune system activation and the migration and infiltration of immune cells caused by vaccines need time.[14,15] Free tumor vaccines may be easily degraded and rapidly metabolized after being injected, so tumor antigens cannot be captured by antigen presenting cells (APCs) in time to trigger expectable anti-tumor immune response.[16–18] Based on the above defects, the study of a new vaccine with sustained release capacity and high antigen delivery efficiency, as well as a direct tumor killing effect, will provide a potential perspective for melanoma immunotherapy.

The tumor cell lysate prepared by freezing and thawing the whole melanoma cell repeatedly contains multiple tumor associated antigens (TAAs) and tumor specific antigens (TSAs).[16–18] Antigen presenting cells (APCs), especially dendritic cells (DCs) are activated after antigens uptake in the peripheral injection site. DCs move to draining lymph nodes through input lymphatic vessels and differentiate into mature DCs (mDCs) in this process, with the up-regulation of major histocompatibility complex (MHC) molecules, costimulatory molecules CD80 and CD86, and adhesion molecules. Subsequently, DCs could present antigen

[a]*Cancer Center, Union Hospital, Tongji Medical College, Huazhong University of Science and Technology, Wuhan, China. E-mail: chenjingwh@hust.edu.cn*

[b]*Department of Neurology, General Hospital of The Yang Tze River Shipping, Wuhan Brain Hospital, Wuhan, China*

[c]*School of Basic Medicine, Tongji Medical College, Huazhong University of Science and Technology, Wuhan, China*

[d]*Orthopaedic Department, General Hospital of Central Theater Command of PLA, Wuhan, China*

[e]*Department of Oncology, Jiangxi Provincial People's Hospital, The First Affiliated Hospital of Nanchang Medical College, Nanchang, China*

[f]*College of Biomedicine and Health and College of Life Science and Technology, Huazhong Agricultural University, Wuhan, China*

[g]*Department of Ophthalmology, Union Hospital, Tongji Medical College, Huazhong University of Science and Technology, Wuhan, China*

[h]*Department of Pediatrics, Renmin Hospital of Wuhan University, Wuhan, China. E-mail: ycz15391569970@163.com*

† These authors contributed equally to this work.

peptides to $CD8^+$ or $CD4^+$ T lymphocytes, thus initiating the specific immune response and achieving the anti-tumor effect.[17] In order to enhance the immunogenicity of tumor vaccines, the addition of an immune adjuvant can strengthen the immune response and promote the anti-tumor effect of vaccine. A synthetic agonist of toll-like receptor 9 (TLR9), cytosine phosphate guanine oligonucleotide (CpG-ODN), is a widely-used vaccine adjuvant which stimulates a variety of immune cells that express TLR9, represented by plasma cell-like dendritic cells (PDCs) and myeloid dendritic cells (MDCs).[19,20]

Recently, tumor vaccines encapsulated by nano-biomaterials, which are more effectively taken up by DCs and improve the delivery efficiency of vaccines, attract great attention from researchers. In previous studies, we synthesized a bioactive melittin–$RADA_{32}$ hydrogel ("MR" hydrogel).[21] We have confirmed that the fusion MR hydrogel showed controllable sustained drug release effect, direct antitumor activity and good biocompatibility, which is an ideal carrier for tumor vaccines.[21–23]

Herein, we encapsulate the immune adjuvant CpG-ODN and tumor cell lysate into the MR hydrogel scaffold to develop a novel vaccine MCL hydrogel. The MR hydrogel not only serves as a drug delivery platform with sustained release capability, but also exhibits attractive tumor killing effect, reducing the tumor burden in the early stage and exposing more tumor antigens. The MCL hydrogel could continuously release tumor antigens and immune adjuvants, recruiting and stimulating the maturation of DCs and promoting the activation of $CD8^+$ or $CD4^+$ T lymphocytes, thereby fully initiating the immune response and achieving a strong anti-tumor effect. This paper confirmed that MCL hydrogels exert a dual anti-tumor effect and served as an efficient immunotherapeutic strategy for melanoma. Our design is shown in Scheme 1.

2 Materials and methods

2.1 Fabrication of the MCL hydrogel

To prepare the whole tumor cell lysate, cultured B16 melanoma tumor cells were suspended in phosphate-buffered saline (PBS) at a concentration of 1×10^7 cells per mL. The cell suspension was rapidly frozen in liquid nitrogen for five minutes and immediately thawed at 37 °C for five minutes. After 5 cycles of freezing and thawing, the suspension was centrifuged at 2000 rpm for ten minutes to discard cell debris. The supernatant was collected and lyophilized to powder. Melittin–$RADA_{32}$ fusion peptide (Ac–RADARADARADARADARADARADARADARADA-GG-GIGAVLKVLTTGLPALISWIKRKRQQ-NH_2, MR peptide) was synthesized by Bankpeptide Ltd (Hefei, China). CpG-ODN (TCGTCGTTTTCGGCGCGCGCCG, from 5′ to 3′) was purchased from U-Me Biotech (Wuhan, China). MR peptide, CpG-ODN and tumor cell lysate powder were first dissolved in sterile deionized water for further use. MR peptide (10 mg mL^{-1}) was dissolved in 0.9% NaCl solution and kept at 4 °C overnight to form the MR hydrogel. The MCL hydrogel was obtained by adding 10% sodium chloride solution to the fully mixed MR/CpG/lysate solution, and the final concentrations of MR, CpG-ODN, tumor cell lysate and NaCl were 10 mg mL^{-1}, 2 mg mL^{-1}, 100 μg mL^{-1}, and 0.9% (w/w), respectively. The mixture was formed by self-assembly through hydrogen bonding between amino acid molecules when kept at 4 °C overnight. All steps were performed under sterile conditions.

2.2 Transmission electron microscopy (TEM) scanning

Transmission electron microscopy (TEM) was used to scan the morphology and structure of MR and MCL hydrogels. To prepare samples for TEM analysis, both hydrogels were diluted with ultrapure water at a ratio of 1 : 20. A drop of hydrogel sample (5 μL) was drop-cast onto a copper grid and incubated for two minutes. Subsequently, the sample was stained with 5 μL of phosphotungstic acid (5%) for thirty seconds followed by drying with a bibulous paper. Then, the grids were imaged by TEM (Titan G2 60–300; FEI Company, OR).

2.3 Sustained release study

500 μL MCL hydrogel was added to a 1.5 mL centrifuge tube, and 500 μL PBS was added on top of the hydrogel layer and was

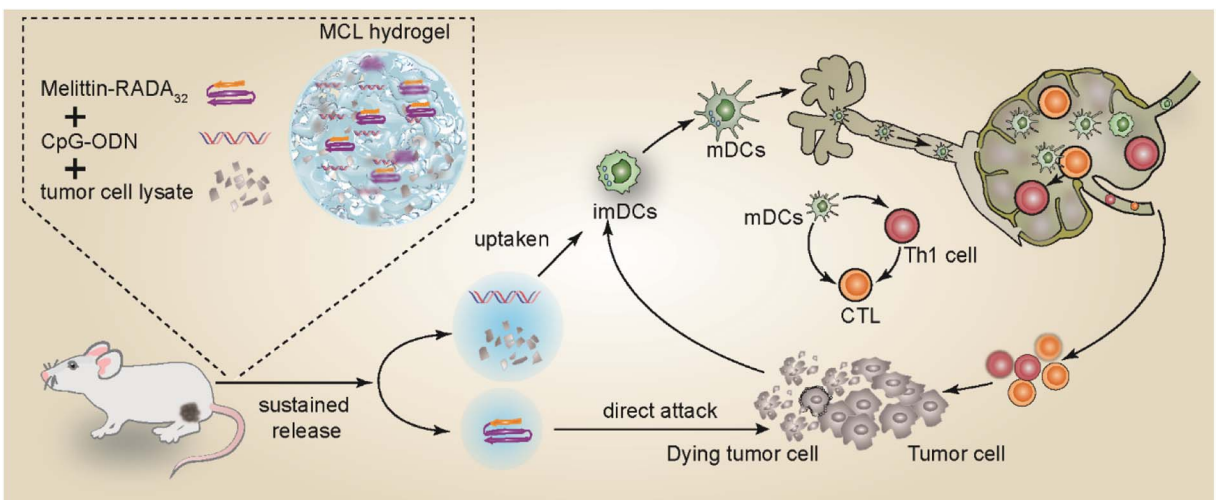

Scheme 1 The fabrication of MCL and the mechanism of MCL-mediated antitumor effects against melanoma.

incubated at 37 °C. Then, the top medium was collected and replaced with fresh PBS at scheduled time points. The concentration of lysate and CpG-ODN in the collected medium was detected by using a MicroBCA™ Protein Assay Kit (Thermo Fisher Scientific, USA) and an Ultramicro spectrophotometer. The release percentage of lysate and CpG-ODN at different time points was calculated.

2.4 Hemolysis assay

The orbital fresh blood of mice was collected to get the red blood cells (RBCs), which was diluted with PBS to 2%. Various concentrations of the MCL hydrogel were added into 500 μL RBC solution in a 1.5 mL centrifuge tube and was incubated at 37 °C for 4 h. Untreated RBC solution was the negative control, and 1% Triton X-100 solution was added into RBC solution as the positive control. After centrifugation at 3000 rpm for ten minutes, the color of supernatant was distinguished and the supernatant was detected by using a microplate reader (Tecan Group Ltd, Mannedorf, Switzerland) at 540 nm.

2.5 Cell culture

B16–F10 cells and B16–luc cells were kindly provided by Professor Zhihong Zhang (HUST, Wuhan, China). B16–F10 and B16–luc cells were maintained in RPMI 1640 medium (Gibco) with 10% fetal bovine serum (Gibco) and 1% antibiotics (Biosharp). Cells were incubated in an atmosphere of 5% carbon dioxide at 37 °C.

2.6 CCK-8 assay

To detect the cytotoxicity of the MCL hydrogel *in vitro*, B16–F10 cells (5000 cells per well) were seeded into a 96-well plate with 100 μL culture medium. After incubation for 24 h, the medium was replaced with 180 μL fresh culture medium and 20 μL MCL hydrogel. After incubation for 24 h at 37 °C, the cell viability was evaluated by the CCK-8 assay.

2.7 Generation and activation of bone marrow-derived DCs (BMDCs)

Bone marrow-derived dendritic cells (BMDCs) were harvested from limb bones of C57BL/6 mice. Limbs were taken out, and the bone marrow was flushed out with RPMI 1640 medium. Then RBCs in the marrow were lysed with RBC lysis buffer. Remaining cells were incubated in RPMI 1640 medium with 20 ng per mL GM-CSF (PeproTech). The medium containing GM-CSF was half refreshed on day 3 and day 5. BMDCs were harvested on day 7. To detect whether BMDCs could be activated by the MCL hydrogel, 100 μL MCL hydrogel was added to BMDCs on day 7. After 24 h incubation, the phenotype of BMDCs was detected by flow cytometry analysis. Cells were harvested and stained for surface markers anti-CD11c (clone N418), anti-CD80 (clone 16-10A1) and anti-CD86 (clone GL-1) for 30 min. Cells were then washed and resuspended in fresh PBS, and analyzed by flow cytometry. A minimum of 10 000 cells were analyzed per condition. All flow cytometry antibodies were purchased from Biolegend.

2.8 Animals

Female C57BL/6 mice (6–8 weeks old) were purchased from HBCDC (Wuhan, China). All animals were raised in a specific pathogen-free (SPF) barrier facility in Tongji Medical College of Huazhong University of Science and Technology (Wuhan, China). All animal procedures were performed in accordance with protocols and experimental guidelines of the Animal Experimentation Ethics Committee approved by the Hubei Provincial Animal Care.

2.9 *In vivo* tumor therapeutic experiments and evaluation of therapeutic effects

1×10^6 B16–F10 cells or B16–luc cells were injected subcutaneously per mouse into the right flank to establish the tumor model. Mice were randomly divided into four groups and were separately treated with 50 μL PBS, CL (50 μL, 2 mg per mL CpG-ODN and 100 μg per mL tumor cell lysate), MR (50 μL, 10 mg mL^{-1}) and MCL (50 μL, 2 mg per mL CpG-ODN + 100 μg per mL tumor cell lysate and 10 mg per mL MR) for tail root injection and another same 50 μL for footpad injection, or 100 μL for peritumoral injection for 3 times on the 7th, 9th, and 13th day. To evaluate the therapeutic efficacy and the safety of treatments, the tumor growth was monitored and calculated every 2 days (the tumor volume = width^2 × length/2). Mice bioluminescence imaging was performed every week. Tumors, inguinal lymph nodes and blood were collected for future analysis.

2.10 *In vivo* tumor prophylactic experiments and evaluation of prophylactic effects

50 μL PBS, CL (50 μL, 2 mg per mL CpG-ODN and 100 μg per mL tumor cell lysate), MR (50 μL, 10 mg mL^{-1}) and MCL (50 μL, 2 mg per mL CpG-ODN + 100 μg per mL tumor cell lysate and 10 mg per mL MR) was subcutaneously injected into the tail root and another same 50 μL into the footpad on day 1, day 3 and day 7. 1×10^6 B16–F10 cells per mouse were inoculated subcutaneously on day 14. The tumor growth was monitored and the tumor volume was calculated every two days. The survival curves and survival percentage were drawn and calculated.

2.11 Flow cytometry

Tumors and lymph nodes of the mice in each group were collected 7 days after the last injection, digested and grinded to single cell suspension. Tumor cell suspension was harvested for tumor-infiltrating T cell (TIL) analysis. TILs were stained with antibodies (Biolegend, USA): anti-CD3 (clone 145-2C11), anti-CD4 (clone GK1.5), and anti-CD8a (clone 53-6.7) for 30 min. To detect intracellular cytokine IFN-γ, tumor cell suspension was incubated with ionomycin (1 mg mL^{-1}; Abcam), phorbol 12-myristate 13-acetate (PMA; 50 ng mL^{-1}, Abcam) and bleomycin (1 mg mL^{-1}; Abcam) for 4–6 h. After that, cells were fixed, permeated and stained with anti-IFN-γ (clone XMG1.2). Popliteal and inguinal lymph node cell suspension were harvested to detect the maturation of DCs. DCs were stained with surface antibodies: anti-CD11c (clone N418), anti-CD80 (clone 16-10A1),

and anti-CD86 (clone GL-1) for 30 min. Cells were then washed and resuspended in fresh PBS, and analyzed by flow cytometry. All flow cytometry antibodies were purchased from Biolegend.

2.12 Statistical analysis

The experimental data were statistically analyzed using GraphPad Prism 7.0 software. The differences between each group were analyzed using one-way ANOVA and the *t*-test. The results were expressed in the form of mean ± SEM. The statistical significance was shown as * for $P < 0.05$; ** for $P < 0.01$; *** for $P < 0.001$, and ns for not significant.

3 Results

3.1 Fabrication and characterization of the MCL hydrogel

We have designed the self-assembled peptide melittin–$RADA_{32}$ (RADARADARADARADARADARADARADARADA–GG–GIGAVLKVLTTGLPALISWIKRKRQQ–NH_2) in a previous article, which was confirmed to be a hydrogel at a concentration of 1% in the presence of 0.9% NaCl (w/w). On this basis, we mixed the tumor cell lysate and CpG-ODN into the MR scaffold to develop the MCL hydrogel. As shown in Fig. 1A, MR was confirmed again to be a hydrogel. The mixture of tumor cell lysate and CpG-ODN

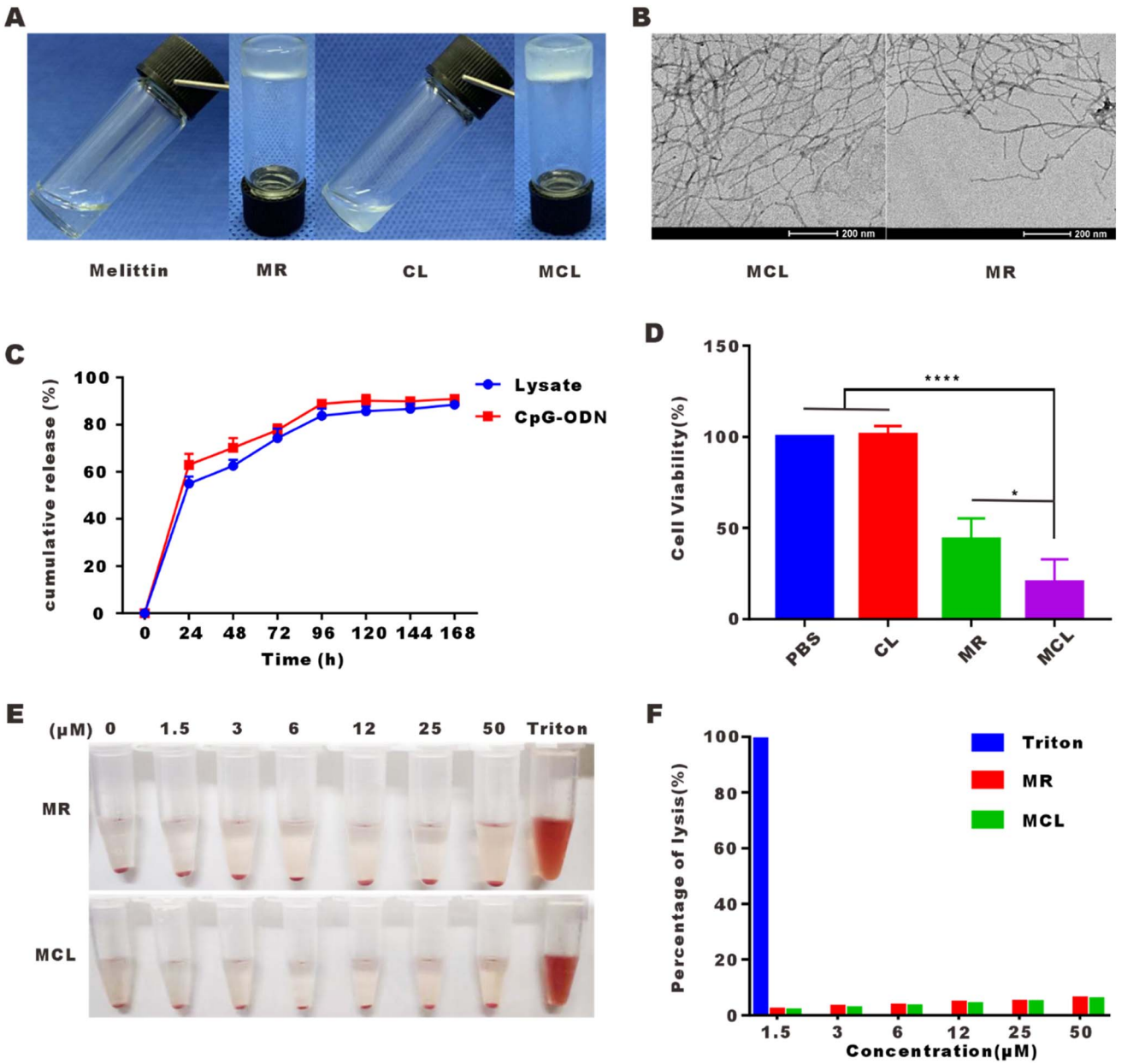

Fig. 1 Fabrication and characterization of the MCL hydrogel. (A) Photographs of melittin solution, MR hydrogel, CL solution and MCL hydrogel. (B) TEM images of the MCL hydrogel and MR hydrogel (the scale bar: 200 nm). (C) Release curves of tumor cell lysate and CpG-ODN from the hydrogel scaffold. (D) The cell viability of B16–F10 cells treated with PBS, CL, MR and MCL for 24 h. Data are shown as mean ± SEM ($n = 6$). (E) Photographs of hemolysis treated with the MR hydrogel and MCL hydrogel. (F) The percentage of hemolysis treated with the MR hydrogel and MCL hydrogel. Data are shown as mean ± SEM ($n = 3$).

was in liquid form. After addition into MR peptide, MCL could be gelled quickly. Moreover, the MR hydrogel was quite a suitable platform to load the tumor vaccine for its nearly 100% encapsulation efficiency, which improved the delivery capability of vaccine.

As can be seen from the TEM images shown in Fig. 1B, MCL and MR hydrogels self-assembled into networks of interwoven nanofibers with diameters of 18.1 ± 3.5 and 11.5 ± 2.3 nm. Whether tumor cell lysate and CpG-ODN can be released by the MR scaffold was detected, and the release curves were shown in Fig. 1C. 54.8% of the tumor cell lysate was released at 24 h, 62.5% at 48 h, and 83.3% at 96 h, while 62.1% of CpG-ODN was released at 24 h, 70.8% at 48 h, and 89.7% at 96 h. From the above, we find that the MCL hydrogel steadily released the cargo, which alleviated the problem of rapid diffusion and degradation of the common liquid vaccine.

To detect the direct cytotoxic effect of the MCL hydrogel on tumor cells, B16–F10 cells were treated with the MCL hydrogel for 24 h and CCK-8 assay was carried out to evaluate the cell viability. As shown in Fig. 1D, the mixture of CpG-ODN and tumor cell lysate (CL) had no cytotoxicity on B16–F10 cells. The MCL hydrogel showed a cell inhibition rate of 79.7%, indicating its direct tumor cell killing capability *in vitro*. The inhibition rate of the MR hydrogel was 58.2%, demonstrating that the

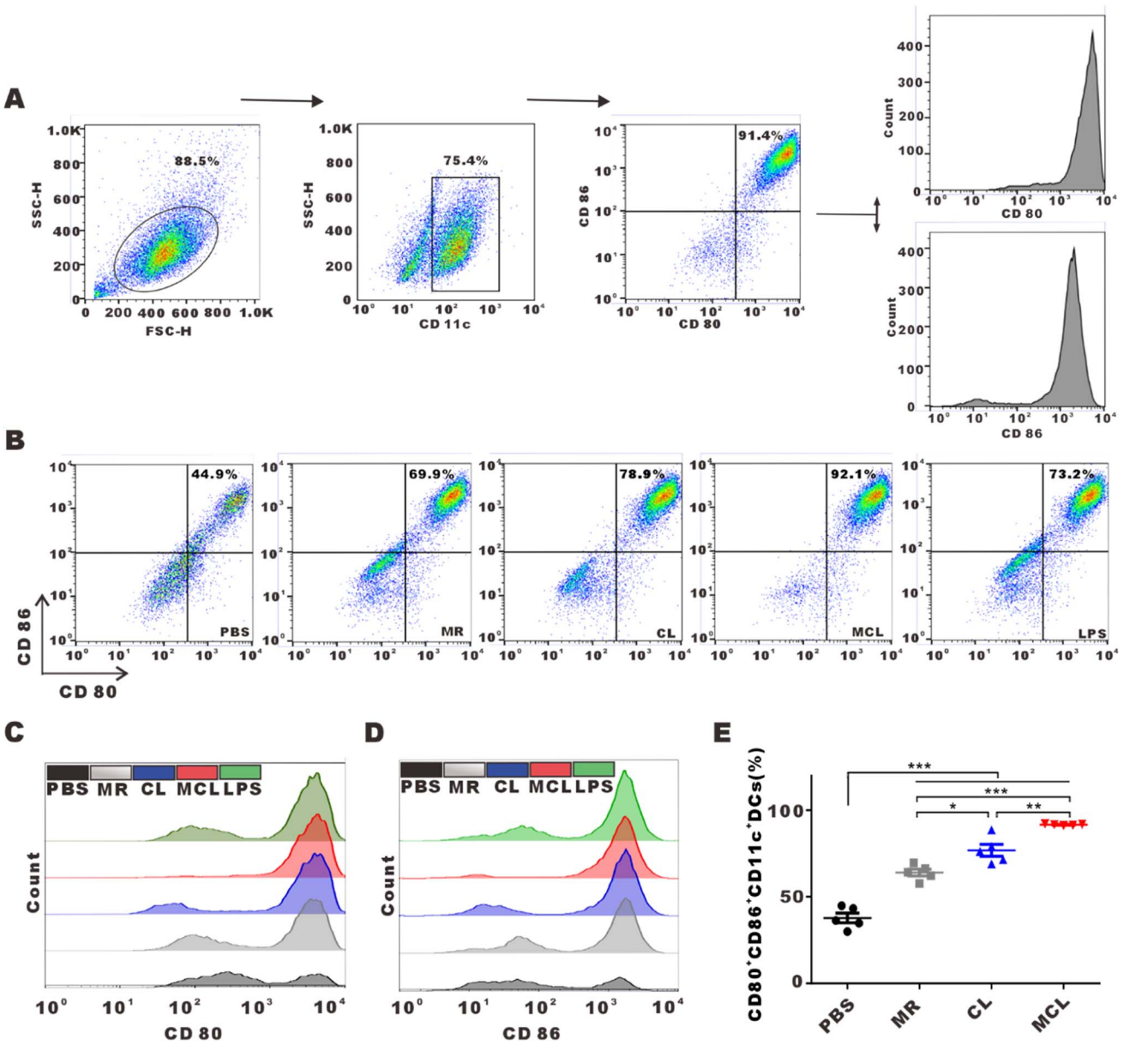

Fig. 2 Activation effects on DCs of MCL *in vitro*. (A) Schematic diagram showing the gating strategy for DCs. (B) Flow cytometry analyses of the percentage of $CD80^+CD86^+$DCs after treatment with PBS, CL, MR, MCL and LPS. LPS serves as the positive control. (C and D) Histograms of CD80 and CD86 expression on BMDCs treated with PBS, CL, MR, MCL and LPS. (E) Statistical analyses of the percentage of $CD80^+CD86^+$DCs in different groups. Data are presented as mean ± SEM ($n = 5$).

encapsulation of CL did not attenuate but enhanced the killing effect of MR. The increased killing effect may rely on melittin inserting into the cell membrane to form pores and the sustained release effect,[24] which may lead to an increased uptake and long-time uptake of CpG-ODN. Andaloussi *et al.* and Luo *et al.* showed that CpG-ODN induced dose-dependent and time-dependent apoptosis of tumor cells.[25,26]

Hemolysis assay was performed to further detect whether the MCL hydrogel eliminates the side effect of strong hemolysis. As displayed in Fig. 1E, we compared the MR hydrogel and MCL hydrogel to 1% Triton X-100 (positive control). The hemolysis rate above 5% is considered as hemolysis. MR and MCL at 50 μM led to a hemolysis rate of 6% and 5.8%, respectively, which confirmed that both MR and MCL hydrogels had little hemolysis effect.

3.2 *In vitro* activation effect on DCs of MCL

We explored whether the release of antigens and CpG-ODN from hydrogels can activate and promote the maturation of DCs. As typical antigen presenting cells, DCs capture antigens, process them and present antigen peptides to $CD8^+$ or $CD4^+$ T cells, and highly express CD80 and CD86. Flow cytometry analysis shown in Fig. 2C and D indicated that BMDCs treated with the MCL hydrogel highly upregulated the expression of CD80 and CD86. We considered the $CD80^+CD86^+$DCs as mature DCs. MR, CL and MCL hydrogel treatment could induce different degrees of DC maturation. The MCL hydrogel showed the strongest capability to stimulate the maturation of DCs (Fig. 2E). Consequently, the MCL hydrogel was capable of potently activating DCs and inducing the maturation of DCs *in vitro*.

3.3 *In vivo* anti-tumor effect of MCL by subcutaneous injection

To explore the anti-tumor effect of MCL *in vivo*, we subcutaneously inoculated B16-Luc cells into C57BL/6J mice. On day 7 post inoculation, these mice were divided into 4 groups and separately treated with 50 μL PBS, CL (50 μL, 2 mg per mL CpG and 100 μg per mL tumor lysate), MR (50 μL, 10 mg ml^{-1}) and MCL (50 μL, 2 mg per mL CpG with 100 μg per mL tumor lysate and 10 mg per mL MR) for tail root injection and another same 50 μL for footpad injection (Fig. 3A). According to the tumor growth curves, the MCL hydrogel group exhibited the strongest antitumor efficacy, with the inhibition rate of 90.7%, while the inhibition rates of MR and CL were 31.0 and 67.6%, respectively (Fig. 3B–G). The tumor growth was also monitored by bioluminescence imaging of B16–luc cells (Fig. 3H and I). Once the tumor volume reached 1000 mm^3, the mice were considered as sacrificed and imaging was no longer performed. Bioluminescence and fluorescence imaging verified that MCL exhibited significant tumor inhibition efficacy. According to the survival curves, mice treated with MCL had the longest survival time compared to PBS, MR and CL (Fig. 3J). Mice treated with PBS all died on the 27th day; all died on the 31st day for MR treatment and on the 41st day for CL treatment. 66.7% of the mice in the MCL group survived for more than 41 days, indicating that MCL prolonged the survival of tumor-bearing mice.

3.4 *In vivo* immune activation effects of the MCL hydrogel

To assess the efficacy of MCL to initiate antitumor immune response *in vivo*, inguinal lymph nodes were collected and mature DCs ($CD80^+CD86^+$DC) were detected by flow cytometry after MCL treatment by subcutaneous injection. The DC maturation rate in the MCL group was 2.8-fold that in the PBS group (Fig. 4A–D). To display the maturation of DCs in lymph nodes by imaging, inguinal lymph nodes were cut into slices to take Opal multispectral fluorescence imaging. CD11c, CD80, CD86 and MHCII were stained with fluorescent antibodies. Sites pointed by arrow showed the high expression of these markers, representing mature DCs in inguinal lymph nodes (Fig. 4E). The average number of $CD80^+CD86^+$DCs in 5 fields of view under a 200× microscope in the MCL group, CL group, MR group and PBS group was 997, 681, 1, and 2, respectively (Fig. 4F). These results indicated that the MCL hydrogel could significantly promote the maturation of DCs *in vivo*.

Adaptive immune responses dominated by cytotoxic T lymphocyte (CTL) and helper T lymphocyte 1 (Th1) are typical effective cells in anti-tumor immunotherapy. To explore whether the novel vaccine MCL further promoted the activation and infiltration of T cells in TME, tumors were collected and filtered into single cell suspension to detect the percentage of T cells by flow cytometry. The proportion of $CD4^+$ T cells in the MCL group, CL group, MR group and PBS group was 37.6 ± 0.7%, 25.9 ± 0.3%, 20.4 ± 1.0% and 17.4 ± 1.1%, respectively. The proportion of $CD8^+$ T cells in the MCL group, CL group, MR group and PBS group was 26.5 ± 0.4%, 16.8 ± 0.3%, 15.9 ± 0.6%, 9.0 ± 0.4%, respectively (Fig. 5B–D). These data showed that MCL obviously promoted the infiltration of $CD4^+$ T cells and $CD8^+$ T cells in TME compared to the other 3 groups. Furthermore, the proportion of effective CTL, defined as $ZIR^-CD45^+CD3^+CD8^+IFN\gamma^+$ cells, in the MCL group was 3.1-fold that in the PBS group (Fig. 5E and F). These results indicated that MCL effectively activated T cell adaptive anti-tumor immune response.

3.5 *In vivo* anti-tumor effect of MCL by peritumoral injection

MCL showed excellent direct antitumor activity *in vitro*, and was further explored for the direct antitumor effect *in vivo*. On day 7 after subcutaneous inoculation of B16–luc cells, mice were randomly divided into four groups and treated with 100 μL PBS, CL (100 μL, 2 mg per mL CpG and 100 μg per mL lysate), MR (100 μL, 10 mg ml^{-1}) and MCL (100 μL, 2 mg per mL CpG with 100 μg per mL lysate and 10 mg per mL MR) by multi-point peritumoral injection to ensure full contact with tumors and exert the direct antitumor effect (Fig. 6A). Similarly, tumor growth curves and bioluminescence imaging were used to monitor tumor growth in each group. The tumor inhibition rates calculated from the tumor volume of the MCL group, CL group and MR group were 99.9%, 91.8% and 50.4%, respectively (Fig. 6B). Not only that, the tumor volume in the MCL group decreased at the early stage from the 1st to the 7th day after

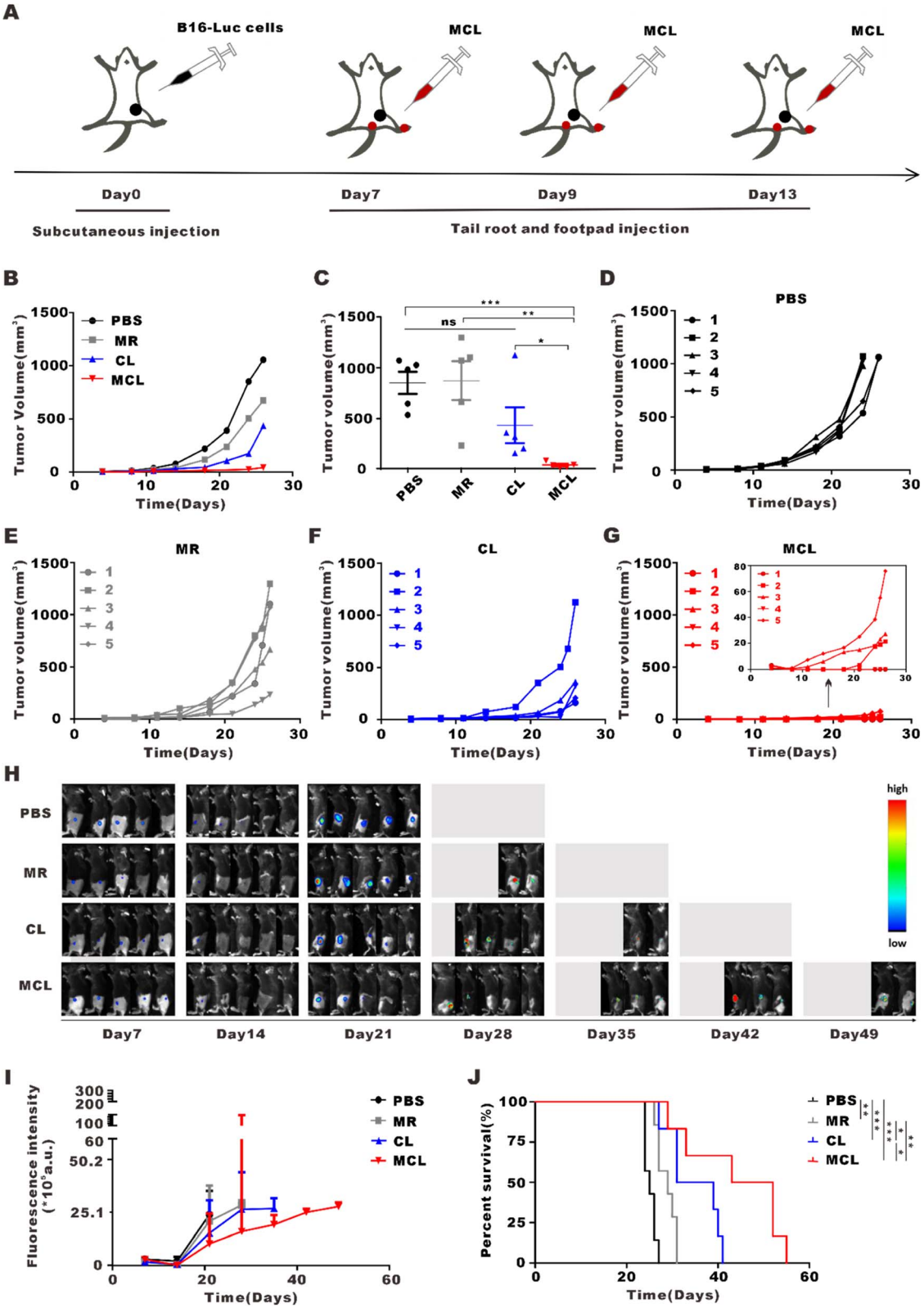

Fig. 3 *In vivo* anti-tumor effects of MCL by subcutaneous injection. (A) Schematic illustration of MCL treatment by subcutaneous injection to inhibit melanoma growth. (B) Tumor growth curves observed after various treatments. (C) Statistical analyses of the tumor volume at the end of observation. Data are shown as mean ± SEM ($n = 5$). (D–G) Tumor growth curves of each mouse in PBS, MR, CL and MCL groups. (H) Bioluminescence images of mice in different groups. (I) Fluorescence intensity curves of mice in different groups. (J) Survival curves of mice in different groups.

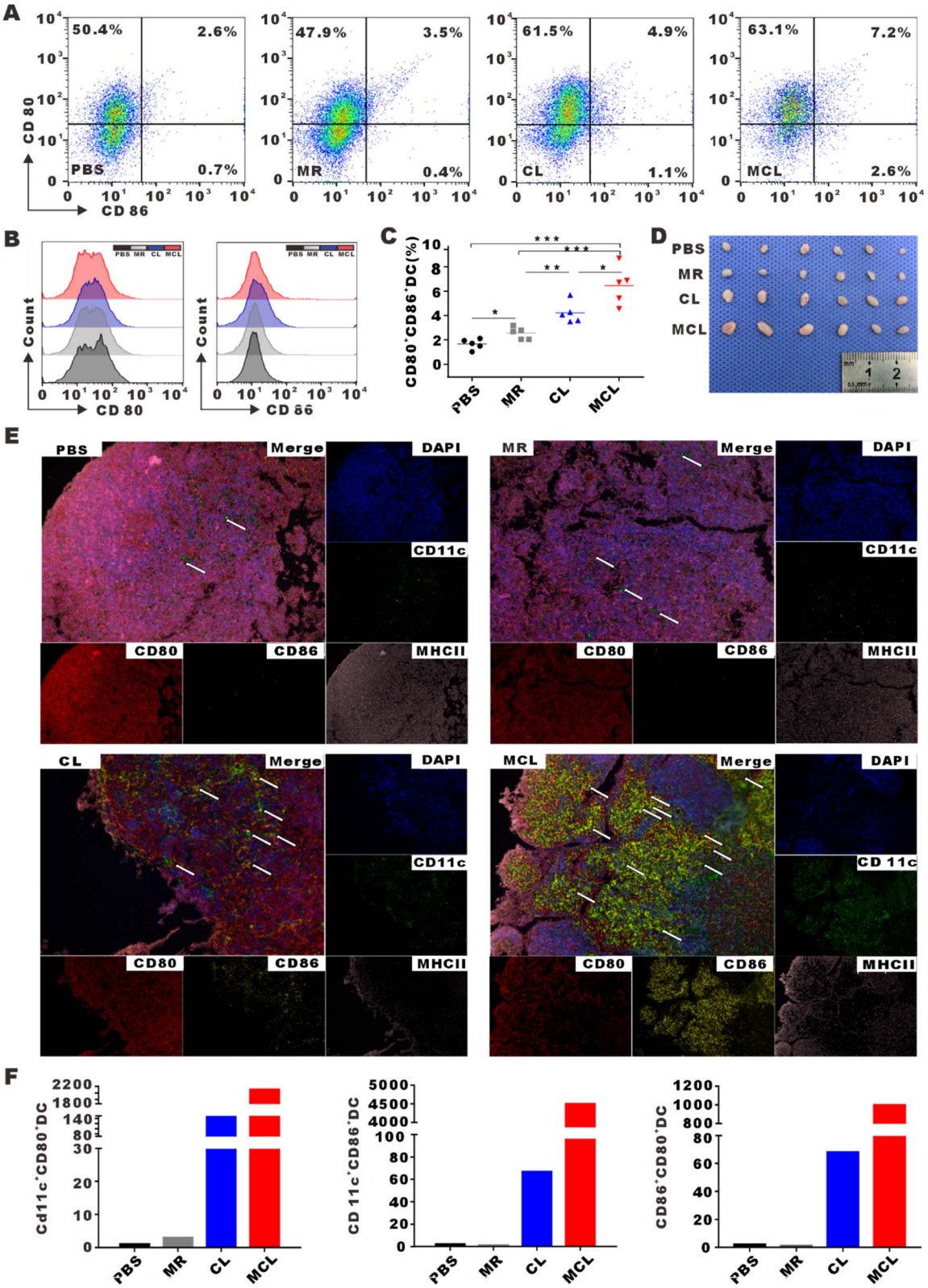

Fig. 4 *In vivo* DC maturation in inguinal lymph nodes induced by MCL. (A and B) Expression of CD80 and CD86 on DCs in inguinal lymph nodes. (C) Statistical analyses of the proportion of $CD80^+CD86^+$DCs. Data are presented as mean ± SEM ($n = 5$). (D) Photographs of inguinal lymph nodes excised from mice in different groups. (E) Opal multispectral fluorescence images of inguinal lymph node slices (blue for DAPI, green for CD11c, red for CD80, yellow for CD86, and pink for MHC II). (F) The average number in 5 fields of vision of $CD11c^+CD80^+$DCs, $CD11c^+CD86^+$DCs and $CD80^+CD86^+$DCs in different groups.

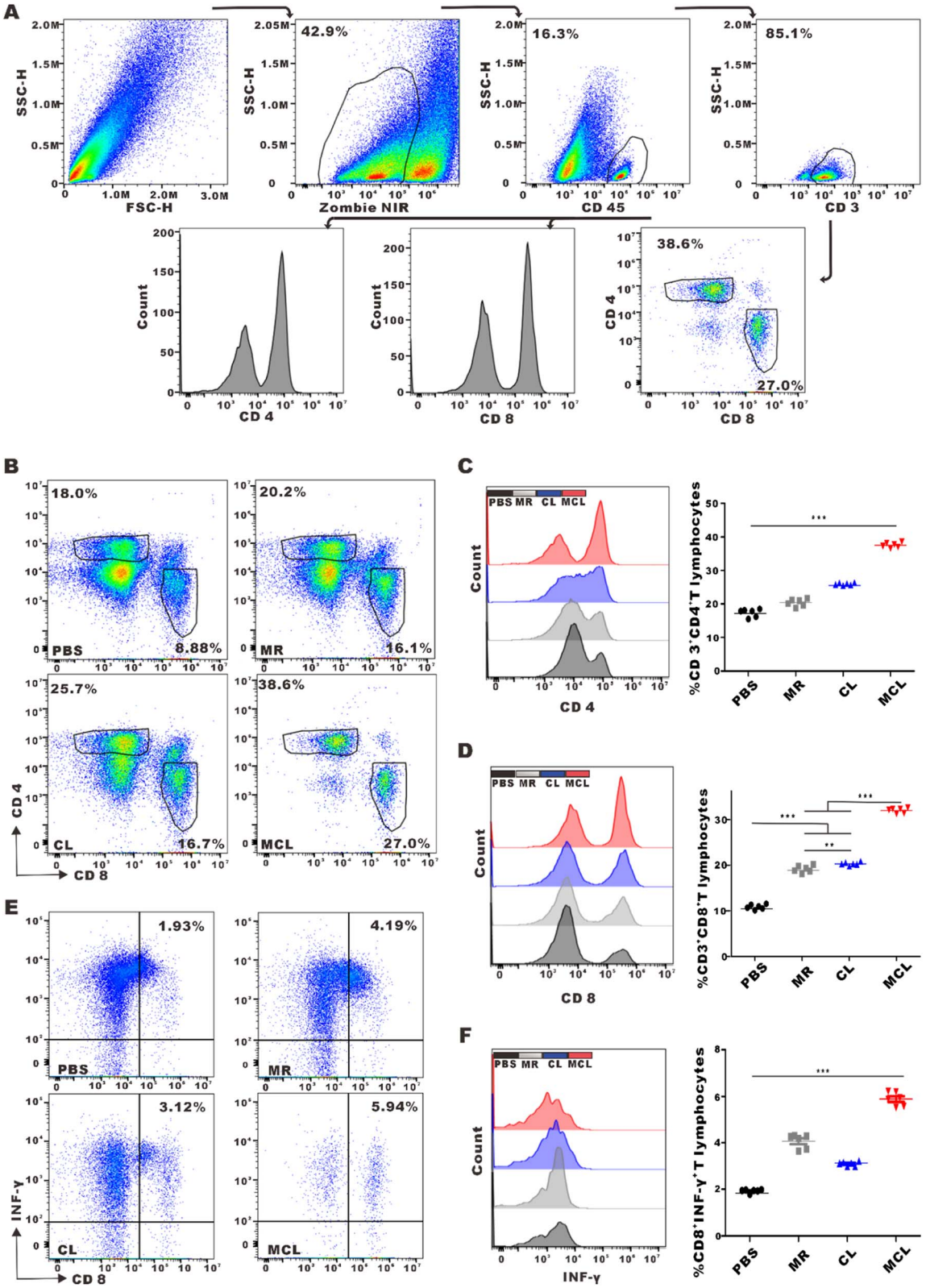

Fig. 5 *In vivo* T cells activation and infiltration in TME induced by MCL. (A) Schematic diagram showing the gating strategy for T cells. (B) The percentage of $CD4^+$T and $CD8^+$T cells in TME. (C). The histograms and statistical analyses of $CD4^+$T cells in different groups. (D) The histograms and statistical analyses of $CD8^+$T cells in different groups. (E) The percentage of $CD8^+$IFN-γ^+T cells in TME. (F) The histograms of IFN-γ expression in $CD8^+$T cells and statistical analyses of $CD8^+$IFN-γ^+T cells in different groups. Data are presented as mean ± SEM ($n = 6$).

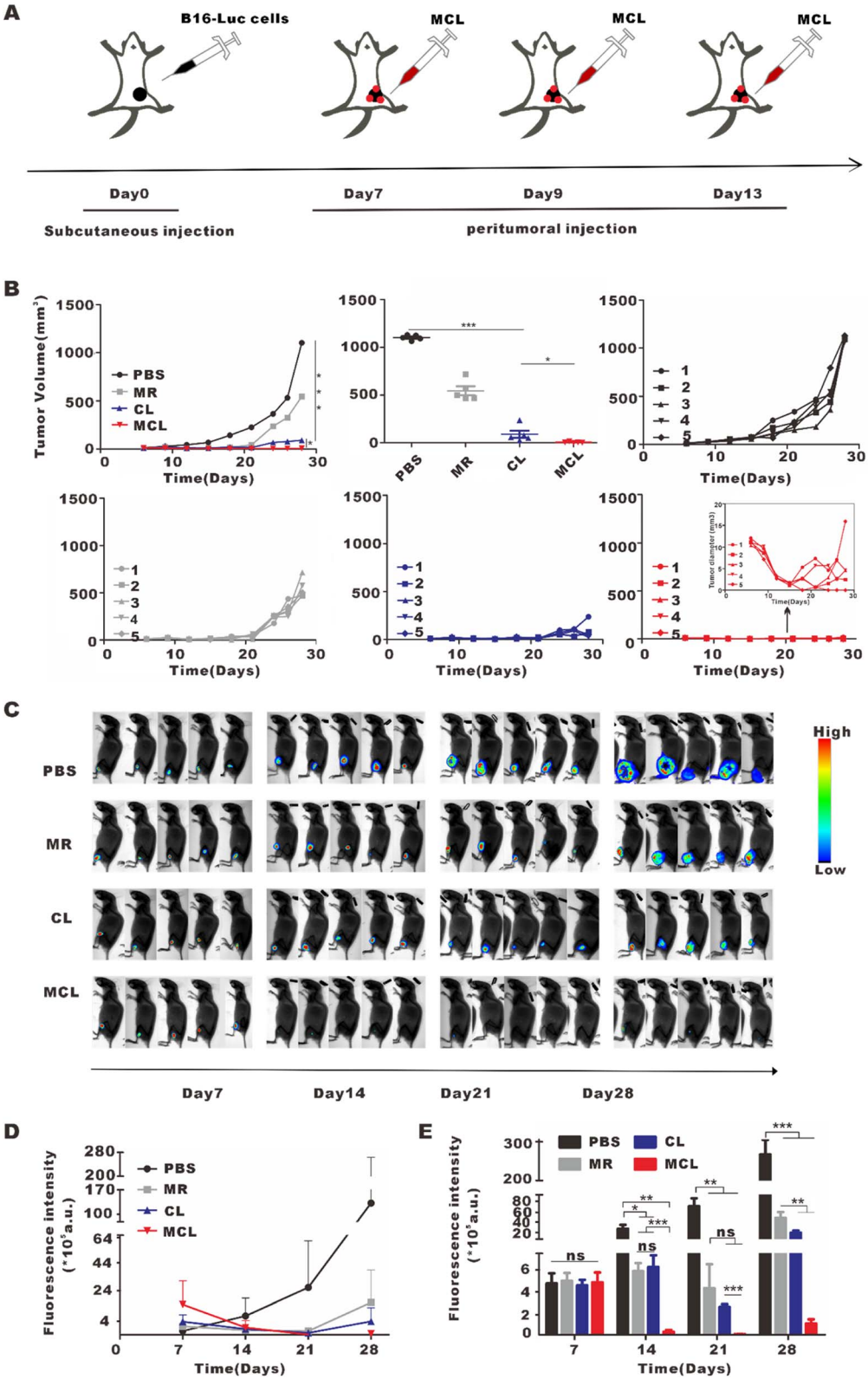

Fig. 6 *In vivo* anti-tumor effect of MCL by peritumoral injection. (A) Schematic illustration of MCL treatment by peritumoral injection to inhibit melanoma growth. (B) Tumor growth curves observed after various treatments. (C) Mice bioluminescence images after various treatments. (D) Fluorescence intensity curves of different groups. (E) Histograms and statistical analyses of fluorescence intensity. Data are shown as mean ± SEM ($n = 5$).

treatment, indicating the direct antitumor activity of MCL. Bioluminescence imaging also showed the lowest mean fluorescence intensity in the MCL group and the diminished luminescence at the first imaging (Fig. 6C–E). Therefore, MCL exhibited a direct antitumor effect *in vivo* to inhibit tumor growth.

3.6 *In vivo* tumor prophylactic effects and biosafety of MCL

Treatments with 50 μL PBS, CL (50 μL, 2 mg per mL CpG and 100 μg per mL tumor lysate), MR (50 μL, 10 mg ml^{-1}) and MCL (50 μL, 2 mg per mL CpG with 100 μg per mL tumor lysate and 10 mg per mL MR) for tail root injection and another same 50 μL for footpad injection were given to mice in advance. After three injections on day 1, day 3 and day 7, we subcutaneously inoculated B16–F10 cells and observed the tumor growth (Fig. 7A). The tumor inhibition rate calculated from the tumor volume of the MCL group, CL group and MR group was 99.4%, 93.9% and 47.0%, respectively (Fig. 7B). The survival analysis showed that the survival percentage of the MCL group, CL group and MR group on the 45th day was 87.5%, 37.5% and 12.5%, respectively, which was about 7 times that of the MR group and 2.5 times that of the CL group. All mice in the PBS group were dead on the 30th day, while those in the MCL group maintained 100% survival (Fig. 7C). These data showed that MCL has potential to effectively prevent tumor growth.

To determine the biosafety of MCL *in vivo*, the body weight and blood biochemical indexes of mice were measured after administration of MCL. The body weight of each group showed similar growth trend rate within the normal range after administration (Fig. 7D). On the 7th day post administration, blood from the orbit was collected to evaluate the function of liver and kidney. Alanine transaminase (ALT), aspartate transaminase (AST), uric acid (UA), blood urea nitrogen (BUN), and creatinine (CR) in the PBS group, MR group, CL group and MCL group were within the normal range, and there was no significant difference between the PBS group and the other groups, indicating the health of the liver and kidney (Fig. 7E). These results confirmed the excellent biosafety of the MCL hydrogel *in vivo*.

4 Discussion

Immunotherapy is the most promising method for advanced melanoma, with few side effects, and prolonged survival. Cancer vaccines, which sensitize the immune system to cancer antigens and induce long-term antitumor immunity, started developing in the 1990s.[27,28] Whole tumor cell lysates contain numerous mutated neoantigens and efficiently promote DC maturation and T cell activation.[29,30] However, they typically activate and expand more $CD4^+$T cells than $CD8^+$T cells.[27] CpG-ODN, an agonist for TLR9 on DCs, can induce DC maturation and the expression of co-stimulatory signals and pro-inflammatory cytokines that promote the activation of cytotoxic $CD8^+$T cells.[27] Therefore, the addition of CpG-ODN further enhances $CD8^+$T cell-mediated antitumor immune response.[31]

With the development of biomedical materials, various drug delivery systems have been continuously studied and applied such as hydrogels, liposomes, nanoparticles, nanotubes, nanoribbons, and micelles.[32,33] Hydrogels exhibit the advantages of efficient drug encapsulation, controllable sustained release performance and excellent biosafety, however, without a direct antitumor or immunomodulatory effect.[14,15] Further development on the use of hydrogels in cancer treatment is needed. Expansion in toxicity to tumor cells and immunomodulatory properties may be attempted.[34] Melittin, the main bioactive component of bee venom, is a cationic peptide composed of 26 amino acids with tumor cell killing capability.[23,35,36] However, its application in anti-tumor treatment is limited because of the hemolytic effect.[21] $RADA_{32}$ is a synthetic amphiphilic peptide which can be self-assembled into interwoven nanofibers in the presence of univalent cations.[22,37] The α-helical conformation of melittin makes it possible to be linked to the polypeptide $RADA_{32}$ through a physical cross-linking method to form the fusion MR hydrogel, which not only achieved the sustained release effect and direct antitumor activity, but also creatively solved the hemolysis caused by systemic administration of melittin.[38] The MR hydrogel could inhibit tumor cell proliferation (with a inhibition rate of 58.2%) and induce DC maturation (with a maturation rate of 69.9%) *in vitro*; as well as a tumor inhibition rate of 50.4% and 1.8-fold of $CD8^+$ T cell infiltration (compared to the PBS group) *in vivo*. Our previous study confirmed the thixotropic nature and good rheological nature of the MR hydrogel. What's more, the MR hydrogel was completely released on day 10 in the presence of proteinase K due to digestion, indicating its excellent biodegradability. The biodistribution of the drug-loading MR hydrogel was imitated by fluorescence dye Cy7. The fluorescence intensity of the MR-Cy7 hydrogel were 4.9 and 7.7-fold that of free Cy7 at 3 and 24 h. These stronger fluorescence signals were also observed on the 3rd and 5th day post-injection, which suggested the enhanced sustained release effect of the MR hydrogel *in vivo*.[21,38] In this paper, we loaded tumor cell lysate and vaccine adjuvant CpG-ODN to the MR scaffold to synthesize the novel cancer vaccine Mellitin–$RADA_{32}$–CpG–Lysate (MCL). The fabrication, antitumor effect and the antitumor mechanism of MCL were explored in this study.

The sustained release effect of MCL was detected by measuring the concentration of protein in lysate and CpG-ODN at different time points. Cumulative release curves demonstrated that the tumor cell lysate and CpG-ODN were steadily released from the hydrogel scaffold, ensuring the sustained drug release over time to inhibit rapid degradation and thus promoting the immune-stimulatory effect. The direct antitumor activity of MCL was verified by CCK-8 assay *in vitro* and melanoma peritumoral administration *in vivo*. This direct killing effect alleviated the tumor burden in the early stage, and also provided more tumor antigens from damaged melanoma cells for the subsequent immune response. The novel hybrid vaccine MCL increased surface markers CD80 and CD86 of BMDCs, and thus promoted DC maturation *in vitro*. After MCL administration by subcutaneous injection *in vivo*, we found that MCL efficiently activated DCs in draining lymph nodes. Flow

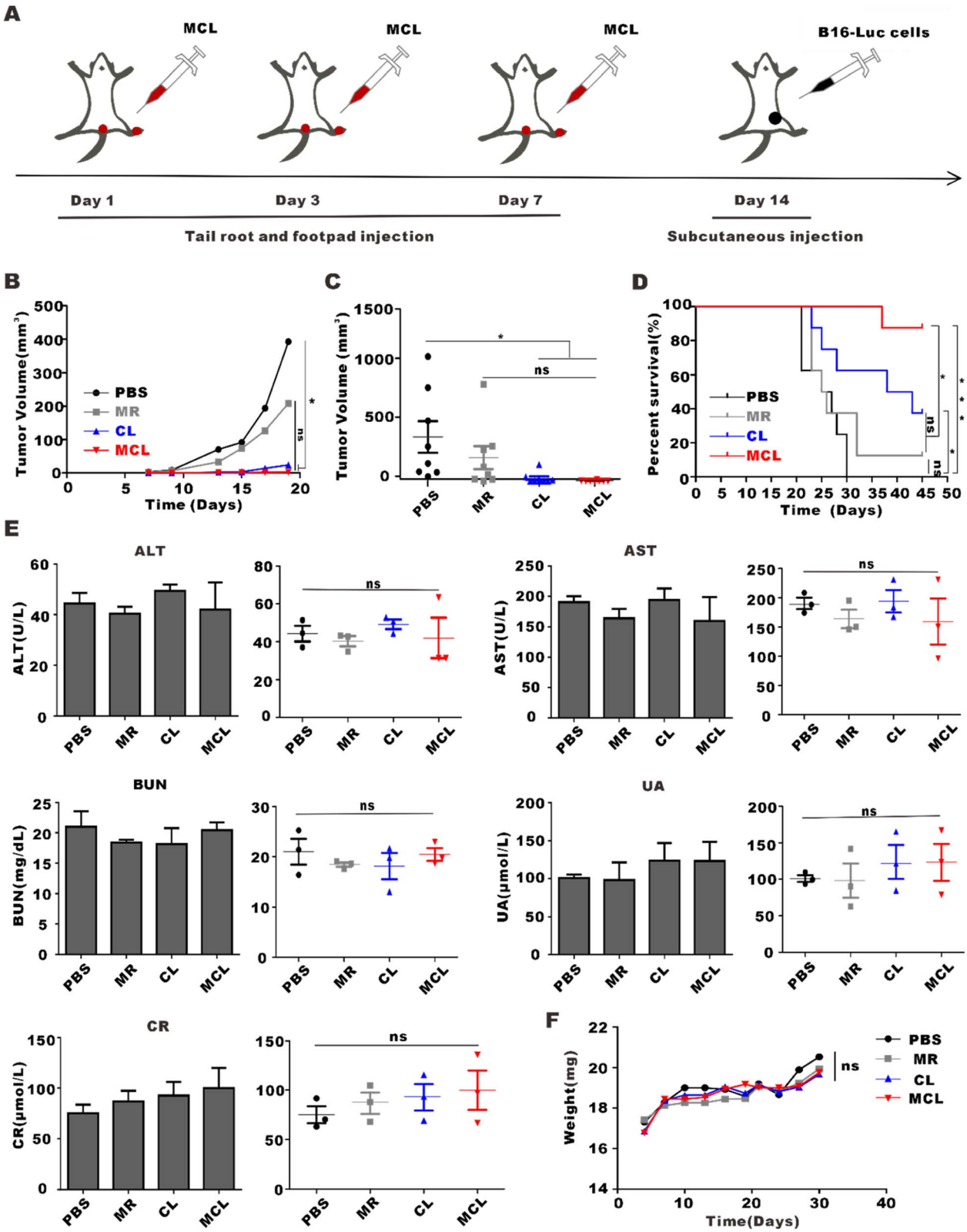

Fig. 7 Prophylactic effects and biosafety of MCL *in vivo*. (A) Schematic illustration of MCL treatment for prophylactic effect on melanoma. (B) Tumor growth curves observed after various treatments. (C) Statistical analyses of the tumor volume at the end of observation. Data are presented as the mean ± SEM ($n = 8$). (D) Survival curves of mice with various treatments. (E) The concentration of AST, ALT, BUN, Cr and UA in blood of mice and the statistical analysis of the data. Data are presented as the mean ± SEM ($n = 3$). (F) Body weight changes of mice after various treatments.

cytometry analyses further showed that MCL could also promote the infiltration of $CD4^+$T cells and $CD8^+$T cells in TME, activated and expanded effector cytotoxic T lymphocytes ($CD8^+IFN\text{-}\gamma^+$ T cells) to mediate antitumor immune response.

MCL efficiently inhibited the growth of melanoma through the anti-tumor immune response and direct killing activity, thus provided a potential strategy for melanoma treatment. In addition, MCL showed the expected prophylactic effects so that the ability to prevent postoperative recurrence of resected cancer can be further explored in further research. In view of the therapeutic and prophylactic effects of MCL on melanoma, as well as its easy preparation and injection, MCL has promising potential in the field of clinical transformation.

5 Conclusion

In summary, a novel tumor vaccine, the MCL hydrogel, comprised of whole tumor cell lysate, adjuvant CpG-ODN and the MR hydrogel scaffold was synthesized in this study. The MCL hydrogel exhibited excellent sustained release character, direct antitumor activity and robust immunostimulatory effects to achieve strong therapeutic and prophylactic effects on melanoma. In mice treated with MCL administration, activated DCs and amplified CTL were detected in inguinal lymph nodes and tumor microenvironment. MCL developed by encapsulating tumor antigens and immune potentiators with an anti-tumor MR hydrogel scaffold holds great promise as a novel cancer vaccine strategy for melanoma treatment.

Ethical statement

All C57BL/6 mice (6–8 weeks old) were purchased from HBCDC (Wuhan, China), and raised in the specific pathogen-free (SPF) barrier facility in Animal Center of Tongji Medical College (Wuhan, China). All animal procedures were performed in accordance with the Guidelines for Care and Use of Laboratory Animals of Tongji Medical College, and approved by the Animal Ethics Committee of Tongji Medical College, Huazhong University of Science and Technology.

Conflicts of interest

There are no conflicts of interest to declare.

Acknowledgements

This work was supported by the National Key R&D Program of China (2021YFC2400600/2021YFC2400602 to JC) and Health Commission of Hubei Province scientific research project (WJ2021Z004).

References

1 D. Schadendorf, D. E. Fisher, C. Garbe, J. E. Gershenwald, J. J. Grob, A. Halpern, *et al.*, Melanoma, *Nat. Rev. Dis. Prim.*, 2015, **1**, 15003.
2 R. Ossio, R. Roldan-Marin, H. Martinez-Said, D. J. Adams and C. D. Robles-Espinoza, Melanoma: a global perspective, *Nat. Rev. Cancer*, 2017, **17**, 393–394.
3 M. A. Davies and K. T. Flaherty, Melanoma in 2017: Moving treatments earlier to move further forwards, *Nat. Rev. Clin. Oncol.*, 2018, **15**, 75–76.
4 E. H. Tracey and A. Vij, Updates in Melanoma, *Dermatol. Clin.*, 2019, **37**, 73–82.
5 W. Li, J. Yan, H. Tian, B. Li, G. Wang, W. Sang, *et al.*, A platinum@polymer-catechol nanobraker enables radio-immunotherapy for crippling melanoma tumorigenesis, angiogenesis, and radioresistance, *Bioact. Mater.*, 2023, **22**, 34–46.
6 J. J. Luke, K. T. Flaherty, A. Ribas and G. V. Long, Targeted agents and immunotherapies: optimizing outcomes in melanoma, *Nat. Rev. Clin. Oncol.*, 2017, **14**, 463–482.
7 E. Feld and T. C. Mitchell, Immunotherapy in melanoma, *Immunotherapy*, 2018, **10**, 987–998.
8 A. Rotte, M. Bhandaru, Y. Zhou and K. J. McElwee, Immunotherapy of melanoma: present options and future promises, *Cancer Metastasis Rev.*, 2015, **34**, 115–128.
9 L. J. Vella, M. C. Andrews, A. Behren, J. Cebon and K. Woods, Immune consequences of kinase inhibitors in development, undergoing clinical trials and in current use in melanoma treatment, *Expert Rev. Clin. Immunol.*, 2014, **10**, 1107–1123.
10 H. Maeng, M. Terabe and J. A. Berzofsky, Cancer vaccines: translation from mice to human clinical trials, *Curr. Opin. Immunol.*, 2018, **51**, 111–122.
11 S. H. van der Burg, Correlates of immune and clinical activity of novel cancer vaccines, *Semin. Immunol.*, 2018, **39**, 119–136.
12 K. K. Wong, W. A. Li, D. J. Mooney and G. Dranoff, Advances in Therapeutic Cancer Vaccines, *Adv. Immunol.*, 2016, **130**, 191–249.
13 T. J. Moyer, A. C. Zmolek and D. J. Irvine, Beyond antigens and adjuvants: formulating future vaccines, *J. Clin. Invest.*, 2016, **126**, 799–808.
14 J. W. Hodge, A. Ardiani, B. Farsaci, A. R. Kwilas and S. R. Gameiro, The tipping point for combination therapy: cancer vaccines with radiation, chemotherapy, or targeted small molecule inhibitors, *Semin. Oncol.*, 2012, **39**, 323–339.
15 A. Bolhassani, S. Safaiyan and S. Rafati, Improvement of different vaccine delivery systems for cancer therapy, *Mol. Cancer*, 2011, **10**, 3.
16 M. Kawahara and H. Takaku, A tumor lysate is an effective vaccine antigen for the stimulation of CD4(+) T-cell function and subsequent induction of antitumor immunity mediated by CD8(+) T cells, *Cancer Biol. Ther.*, 2015, **16**, 1616–1625.
17 G. N. Shi, C. N. Zhang, R. Xu, J. F. Niu, H. J. Song, X. Y. Zhang, *et al.*, Enhanced antitumor immunity by targeting dendritic cells with tumor cell lysate-loaded chitosan nanoparticles vaccine, *Biomaterials*, 2017, **113**, 191–202.
18 H. Song, P. Huang, J. Niu, G. Shi, C. Zhang, D. Kong, *et al.*, Injectable polypeptide hydrogel for dual-delivery of antigen and TLR3 agonist to modulate dendritic cells in vivo and

enhance potent cytotoxic T-lymphocyte response against melanoma, *Biomaterials*, 2018, **159**, 119–129.
19 S. Iho, J. Maeyama and F. Suzuki, CpG oligodeoxynucleotides as mucosal adjuvants, *Hum. Vaccines Immunother.*, 2015, **11**, 755–760.
20 J. Vollmer and A. M. Krieg, Immunotherapeutic applications of CpG oligodeoxynucleotide TLR9 agonists, *Adv. Drug Delivery Rev.*, 2009, **61**, 195–204.
21 H. Jin, C. Wan and Z. Zou, Tumor Ablation and Therapeutic Immunity Induction by an Injectable Peptide Hydrogel, *ACS Nano*, 2018, **12**, 3295–3310.
22 F. Gelain, L. D. Unsworth and S. Zhang, Slow and sustained release of active cytokines from self-assembling peptide scaffolds, *J. Controlled Release*, 2010, **145**, 231–239.
23 C. E. Dempsey, The actions of melittin on membranes, *Biochim. Biophys. Acta*, 1990, **1031**, 143–161.
24 X. Dai, J. Meng, S. Deng, L. Zhang, C. Wan, L. Lu, *et al.*, Targeting CAMKII to reprogram tumor-associated macrophages and inhibit tumor cells for cancer immunotherapy with an injectable hybrid peptide hydrogel, *Theranostics*, 2020, **10**, 3049–3063.
25 Y. Luo, X. Fu, R. Ru, B. Han, F. Zhang, L. Yuan, *et al.*, CpG Oligodeoxynucleotides Induces Apoptosis of Human Bladder Cancer Cells via Caspase-3-Bax/Bcl-2-p53 Axis, *Arch. Med. Res.*, 2020, **51**, 233–244.
26 A. El Andaloussi, A. M. Sonabend, Y. Han and M. S. Lesniak, Stimulation of TLR9 with CpG ODN enhances apoptosis of glioma and prolongs the survival of mice with experimental brain tumors, *Glia*, 2006, **54**, 526–535.
27 M. Kwak, K. M. Leick, M. M. Melssen and C. L. Slingluff Jr, *Vaccine Strategy in Melanoma*, Surgical Oncology Clinics of North America, 2019, vol. 28, pp. 337–351.
28 L. E. Davis, S. C. Shalin and A. J. Tackett, Current state of melanoma diagnosis and treatment, *Cancer Biol. Ther.*, 2019, **20**, 1366–1379.
29 Z. Hu, P. A. Ott and C. J. Wu, Towards personalized, tumour-specific, therapeutic vaccines for cancer, *Nat. Rev. Immunol.*, 2018, **18**, 168–182.
30 R. Zhang, M. M. Billingsley and M. J. Mitchell, Biomaterials for vaccine-based cancer immunotherapy, *J. Controlled Release*, 2018, **292**, 256–276.
31 D. M. Klinman, Immunotherapeutic uses of CpG oligodeoxynucleotides, *Nat. Rev. Immunol.*, 2004, **4**, 249–258.
32 H. Acar, S. Srivastava, E. J. Chung, M. R. Schnorenberg, J. C. Barrett, J. L. LaBelle, *et al.*, Self-assembling peptide-based building blocks in medical applications, *Adv. Drug Delivery Rev.*, 2017, **110–111**, 65–79.
33 M. S. Ekiz, G. Cinar, M. A. Khalily and M. O. Guler, Self-assembled peptide nanostructures for functional materials, *Nanotechnology*, 2016, **27**, 402002.
34 J. Zhou, C. Wan, J. Cheng, H. Huang and J. F. Lovell, Delivery Strategies for Melittin-Based Cancer Therapy, *ACS Appl. Mater. Interfaces*, 2021, **13**, 17158–17173.
35 B. Bechinger, Structure and functions of channel-forming peptides: magainins, cecropins, melittin and alamethicin, *J. Membr. Biol.*, 1997, **156**, 197–211.
36 H. Raghuraman and A. Chattopadhyay, Melittin: a membrane-active peptide with diverse functions, *Biosci. Rep.*, 2007, **27**, 189–223.
37 H. Jin, G. Zhao, J. Hu, Q. Ren, K. Yang and C. Wan, Melittin-Containing Hybrid Peptide Hydrogels for Enhanced Photothermal Therapy of Glioblastoma, *ACS Appl. Mater. Interfaces*, 2017, **9**, 25755–25766.
38 Y. Zhou, T. Ye, C. Ye, C. Wan, S. Yuan, Y. Liu, *et al.*, Secretions from hypochlorous acid-treated tumor cells delivered in a melittin hydrogel potentiate cancer immunotherapy, *Bioact. Mater.*, 2022, **9**, 541–553.